ORIGINAL PAPER

Improved electrochemical performance of Li[Li$_{0.2}$Mn$_{0.54}$Ni$_{0.13}$Co$_{0.13}$]O$_2$ by doping with molybdenum for Lithium battery

Jiangyong Du · Zhongqiang Shan · Kunlei Zhu · Xiaoyan Liu · Jianhua Tian · Haiyan Du

Abstract The Li[Li$_{0.2}$Mn$_{0.54}$Ni$_{0.13}$Co$_{0.13}$]O$_2$ materials doped with different Mo content were studied using electron microscopy (SEM), transmission electron microscopy (TEM), energy dispersive X-ray analysis (EDX), and X-ray diffractometry (XRD). The electrochemical properties were also measured. An increase of Mo content resulted in a bigger lattice volume and a lower cation disorder. In addition, the electrochemical performance was enhanced with the increasing Mo content. However, more aggregation of particles was found to occur at a higher Mo content, which resulted in worse electrochemical performance. The highest electrochemical performance was obtained with a 5 mol% Mo addition.

Keywords Cathode materials · Structure · Mo · Capacity

Introduction

Over the past few years, much work has been performed on the structures and properties of layered lithium cobalt nickel manganese oxide materials because they are seen to be promising cathode materials for Li-ion batteries in terms of their abundance, low-cost, and nontoxicity [1–5]. Among all these, Mn-based lithium-rich layered oxides are more attractive due

J. Du · Z. Shan · K. Zhu · X. Liu · J. Tian
School of Chemical Engineering and Technology, Tianjin University, Weijin Road 92#, Tianjin 300072, People's Republic of China

J. Du
e-mail: dujiangyong@126.com

H. Du (✉)
Key Laboratory of Advanced Ceramics and Machining Technology of Ministry of Education, School of Materials Science and Engineering of Tianjin University, Weijin Road 92#, Tianjin 300072, People's Republic of China
e-mail: hydu@tju.edu.cn

to the high theoretical specific capacity and relative low cost. The successful application of these materials can increase the energy density of Li-ion batteries, such as Li$_{1.2}$Mn$_{0.54}$Ni$_{0.13}$Co$_{0.13}$O$_2$, which shows a more than 250 mAh g^{-1} capacity when the rate is 0.1 C [5–9]. Recently, this cathode material has seen more interest in research within the electrode material field. Zhao and Lee [5, 10] studied the effect of lithium, manganese and nickel content on the electrochemical performance. Many people [4, 6, 11–13] have improved this cathode material through various methods. However, for practical applications of this solid solution material as lithium-ion battery cathodes, the electrochemical performance needs to be improved, especially for the development of electric vehicles. On the other hand, the radius of the lithium ion (r_{Li^+}=0.76 nm) is close to the radius of the nickel ion ($r_{Ni^{2+}}$=0.69 nm). Therefore, the cation disorder tends to happen between the nickel ions and lithium ions [14]. The higher cation disorder would make it more difficult for lithium ions to deintercalate from the layered structure, resulting in a loss of electrochemical performance. So the content of Ni can affect the electrochemical performance of the layered lithium–cobalt–nickel–manganese–oxide materials dramatically. Therefore, the modification on nickel may improve structural ordering and electrochemical performance. The Mo has a larger atomic radius than Mn, Ni and Co, the strong Mo–O hybridization may replace the weak Ni–O hybridization, which may reduce the cation disorder and enhance metallic behaviors. The effects of Mo on the structure of the layered lithium cobalt nickel manganese oxide materials should be larger than nickel. Therefore, the molybdenum was hoped to improve the structure properties of the layered lithium cobalt nickel manganese oxide materials.

The doping other compounds or elements into the cathode materials, such as K, F, Na, Mo, etc. [6, 15–17], has been studied by many people. This method can change both structure and/or morphology, as the doped elements enter into the

crystal lattice of the cathode materials. The lattice parameters may be also changed after the crystal lattice has had more kinds of elements. The structure may be improved after doping, and the electrochemical properties will also then be improved. The cathode materials doped by Mo have also been widely studied [17–21]. They have proved the advantage of the large radius of molybdenum atom. However, they did not report the optimal amount of Mo for doping lithium-rich layered cathode materials or the impact on the particle size. Here, supposed that the doping modification would improve the structure, lower the cation disorder and enhance the electrochemical performance of the cathode material $Li_{1.2}Mn_{0.54}Ni_{0.13}Co_{0.13}O_2$. Lastly, through this study it is hoped to find out the optimal amount of Mo for doping lithium-rich layered cathode materials, the impaction on the particle size.

In this work, a series of $Li[Li_{0.2}Mn_{0.54}Ni_{0.13-x}Co_{0.13}Mo_x]O_2$ (x=0, 0.01, 0.03, 0.05, 0.07, and 0.09) materials were prepared, and the effects of Mo doping on the structure, morphology, and electrochemical performance of the $Li_{1.2}Mn_{0.54}Ni_{0.13}Co_{0.13}O_2$ cathode materials were compared. The SEM, TEM, and XRD were employed to investigate the effect and mechanism of doping.

Experiment

The $Li_{1.2}Mn_{0.54}Ni_{0.13}Co_{0.13}O_2$ (LLNCM) materials were prepared via a calcination process for mixed transition metal hydroxide precursor obtained by a supersonic co-precipitation method. Stoichiometric amounts of $Mn(Ac)_2$, $Ni(Ac)_2$ and $Co(Ac)_2$ were dissolved in de-ionized water and kept at 50 °C with continuous magnetic stirring. Then LiOH solution was then added to the mixed solution until the pH value was above 8. A supersonic-wave treatment (200 or 950 kHz) and 300 W was applied in all above processes. The precipitated mixed hydroxide was then filtered, washed thoroughly with de-ionized water and lastly dried at 120 °C overnight.

The obtained precursor mixed with stoichiometric amounts of Li_2CO_3 and various stoichiometric amounts of ammonium heptamolybdate ($(NH_4)_6Mo_7O_{24}\cdot4H_2O$) were made into pellets and pre-calcined at 500 °C for 15 h, then ground and pressed into new pellets. The target materials were finally gained by sintering the new pellets at 900 °C for 3 h and then allowing them to cool down to room temperature.

The cathode electrodes were prepared using a slurry coating procedure. The slurry consisting of 80 wt% as-prepared materials, 10 wt% carbon conductive agent (acetylene black), and 10 wt% polyvinylidene fluoride (PVDF) was coated on aluminum foil, then kept at 120 °C overnight in vacuum. Lithium foil served as the anode electrode, 1 M LiPF6 in ethylene carbonate (EC)-dimethyl carbonate (DMC) (1:1 in

volume) was used as the electrolyte, and a polypropylene micro-porous film (Cellgard 2300) as the separator.

The crystalline structure analysis of these cathode materials were carried out by X-ray diffraction (XRD) with a Rigaku D/MAX-2500 (Rigaku,Japan) diffractometer equipped with Cu Kα radiation. The lattice parameters were refined by the Rietveld method with General Structure Analysis Software (GSAS program, Los Alamos National Laboratory, USA). The morphology of the cathode materials was investigated by scanning electron microscopy (SEM, HITACHI, S-4800) and high-resolution transmission electron microscopy (HRTEM, TECANI G2 F20, FEI Company).

Electrochemical behaviors of the samples were examined using CR2032type coin cell with two electrodes. Galvanostatic charge–discharge method was performed on a LAND CT-2001A system between 2.0 and 4.8 V at room temperature. Capacities were calculated by only considering the active mass of the electrodes. The fabricated cells were tested at different current density. Electrochemical impedance spectroscopies (EIS) were measured on Zahner IM6e electrochemical workstation (Germany) in the frequency range of 1, 000 kHz–00 mHz at a disturbance amplitude of ±5 mV. The EIS results were simulated using ZPVIEW software.

Results and discussion

Structure of the cathode material

The chemical compositions of the obtained samples were investigated by ICP. It was found that the final products could only be written as $Li_{1.21}Mn_{0.538}Ni_{0.129}Co_{0.131}O_x$, $Li_{1.19}Mn_{0.541}Ni_{0.116}Co_{0.131}Mo_{0.01}O_x$, $Li_{1.22}Mn_{0.543}Ni_{0.093}Co_{0.132}Mo_{0.028}O_x$, $Li_{1.2}Mn_{0.54}Ni_{0.08}Co_{0.128}Mo_{0.046}O_x$, $Li_{1.19}Mn_{0.54}Ni_{0.062}Co_{0.131}Mo_{0.065}O_x$, and $Li_{1.21}Mn_{0.54}Ni_{0.039}Co_{0.13}Mo_{0.087}O_x$, when the doping levels of Mo at Ni site are 0, 0.01, 0.03, 0.05, 0.07, and 0.09, respectively.

The SEM images, particle size distributions and EDX patterns of the cathode materials are shown in Fig. 1. All of them are magnified same times. The SEM images of the composite cathodes reveal that all powders are comprised of well crystallized particles with obvious edges and smooth facets. The particle sizes and particle size distributions exhibit differences for all samples. The pristine samples show nearly the same particle size, mainly distributed around 150 nm. With the increasing of Mo, the particles grew into agglomeration, and their size increased. At the same time, the particle size distributions became wider. The particle size of cathode materials may have impacts on electrochemical performance. As the particle size increases, the transport path of lithium ion would become longer, which would then impact the kinetic

Fig. 1 The SEM images, particle size distributions and EDX patterns of cathode materials of (*a*) *x*=0; (*b*) *x*=0.01; (*c*) *x*=0.03; (*d*) *x*=0.05, (*e*) *x*=0.07, (*f*) *x*=0.09
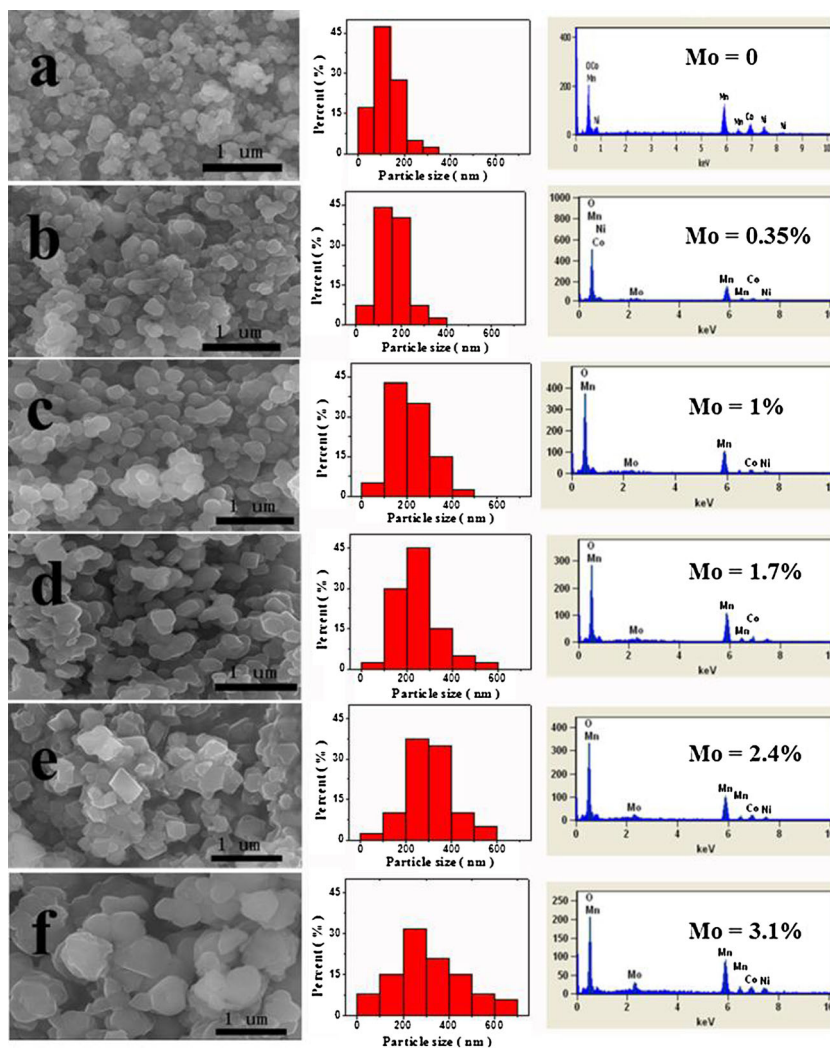
properties of electrodes to some extent, leading to a lower capability [22]. The bigger the particle size is, the worse electrochemical properties it has.

Their mean particle sizes and content of Mo are shown in Table 1. Their mean particle sizes increase from 0.12 μm (pristine) to 0.37 μm (0.09). Such consecutive changes in the particle size are believed to be associated with the doped Mo. This agglomeration appears to be the primary reason for worse electrochemical performance. The EDX results are displayed in Table 1. For each *x* value, the elemental content of Mo is close to the stoichiometric value of *x* (Table 1). This means that the as-prepared samples series can be

approximately described as $Li[Li_{0.2}Mn_{0.54}Ni_{0.13-x}Co_{0.13}Mo_x]O_2$ according to that of the corresponding raw materials.

The XRD patterns of LLNCM before and after being improved by Mo are shown in Fig. 2. As shown in Fig. 2, among these diffraction peaks, the strong peaks can be indexed as the layered α-NaFeO$_2$ structure using the space group R$\overline{3}$ m which is ordinarily taken as the signature of LiMO$_2$ (M=Li$_{0.2}$Mn$_{0.8}$ and/or Ni$_{0.33}$Co$_{0.33}$Mn$_{0.33}$) phase. The weak diffraction peaks in the 2θ range of 20°~25° belong to the super lattice ordering characteristics for the periodic occupation of Li$^+$ ions in the transition metal layers of a LiMO$_2$ lattice unit, which prove the coexistence of the component Li$_2$MnO$_3$ in the homogeneous crystal phases of these cathode materials. Clear separation of adjacent peaks of (006)/(012) and (108)/(110) indicates that the samples have a well crystalline layered structure [23–27]. As seen in the work done by Wang et al. [28, 29], the intensity ratio of the (003) to (104) peak ($I_{(003)}/I_{(104)}$), and the lattice parameter ratio of *c* to *a* (*c*/*a*) can be used to measure the layered structure and

Table 1 Mean sizes and Mo contents of samples

x value	pristine	0.01	0.03	0.05	0.07	0.09
Mean size (um)	0.12	0.16	0.20	0.24	0.31	0.37
Mo contents (%)	0	0.96	2.93	4.86	6.91	8.89

Fig. 2 The XRD patterns of $Li_{1.2}Mn_{0.54}Co_{0.13}Ni_{0.13}O_2$ before and after doping with various amounts of Mo
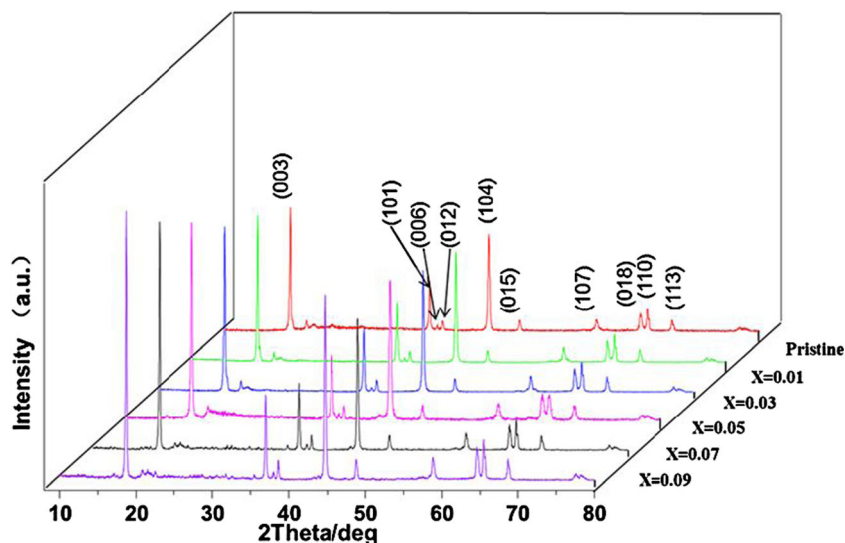
cation disorder, the higher value of c/a (or, $I_{(003)}/I_{(104)}$) meaning better layered structural ordering and lower cation disorder.

Rietveld refinements within R-3m phase were used by GSAS software to investigate the variations from the view of lattice parameters. Table 2 shows the refinement results and the ratios of c/a, $I_{(003)}/I_{(104)}$. The lattice constant a in the unit cell slightly increases from 2.86130 Å (pristine) to 2.86368 Å (0.09), whereas, the lattice constant c gradually decreases from 14.2816 Å (pristine) to 14.2740 Å (0.09). The lattice volume, on the other hand, is seen to slightly increase from 101.224 Å^3 (pristine) to 101.375 Å^3 (0.09). Such consecutive changes in the unit cell of layered lattice are believed to be associated with the improvement as brought about by Mo. In addition, the intensity ratio of the (003) to (104) peak ($I_{(003)}/I_{(104)}$) gets larger, and the lattice parameter ratio of c to a (c/a) gets smaller with the increase of Mo. The increasing of the intensity ratio of the (003) to (104) peak ($I_{(003)}/I_{(104)}$) means that the cation disorder got lower. The lattice parameter ratio of c to a (c/a) decreasing means that the layered structural ordering improved. Thus, the Mo can improve the structure of the cathode materials.

TEM is also employed to investigate the atomic changes of the LLNCM after doping. As shown in Fig. 3a, the low-magnification TEM bright field image reveals the agglomeration effects and smooth facets of crystallized LLNCM particles. The electron diffraction pattern corresponding to Fig. 3a is shown in Fig. 3b. According to the rings of electron diffraction, it could be concluded that the LLNCM is a solid solution [30]. Additionally, in view of the surface areas shown in HRTEM image of Fig. 3c and the fast Fourier transformation (FFT), inverse fast Fourier transformation (IFFT) to Fig. 3c, the LLNCM have a well-formed layered structure. The lattice fringe is 4.76 Å which corresponds to the (003) planes. The FFT and IFFT in Fig. 3e are shown in Fig. 3f. Figure 3f corresponds to rhombohedral phase. The Fig. 3d, f prove the coexistence of two phases, layered (monoclinic) and rhombohedral.

Electrochemical properties

The first charge/discharge curves of cathode materials at the current density of 20 mA g^{-1}, between 2.0 and 4.8 V are shown in Fig. 4. Among these cathode materials, the composite cathodes with $x=0.05$ has the largest initial charge and discharge capacity of 420 and 296.8 mAh g^{-1}, respectively. The composite cathodes without any Mo have the worst electrochemical properties. With increases of the content of Mo, the charge and discharge capacity increases first and then decreases. This phenomenon may be caused by the structure and particle size. The better structure makes the electrochemical properties get better; however, the bigger particle size also makes the electrochemical properties get worse. With the increase of the content of Mo, the structure gets better, the lattice volume gets bigger, and the particle size gets bigger. The electrochemical properties are mainly impacted by structure and lattice volume, when the x value is below 0.05. The

Table 2 Lattice parameters of $Li_{1.2}Mn_{0.54}Co_{0.13}Ni_{0.13}O_2$ before and after doping with various amounts of Mo

Mo(x)	a(Å)	b(Å)	c(Å)	c/a	$I_{(003)}/I_{(104)}$	V(Å^3)
0	2.8613	2.8613	14.2816	4.9913	1.25	101.2591
0.01	2.8627	2.8627	14.2805	4.9885	1.34	101.3505
0.03	2.8630	2.8630	14.2792	4.9875	1.37	101.3625
0.05	2.8632	2.8632	14.2773	4.9865	1.41	101.3635
0.07	2.8635	2.8635	14.2755	4.9853	1.55	101.3716
0.09	2.8637	2.8637	14.2740	4.9845	1.72	101.3751

Fig. 3 TEM identification of $Li_{1.2}Mn_{0.54}Ni_{0.04}Co_{0.13}Mo_{0.09}O_2$. **a** Low magnification TEM bright field image. **b** Electron diffraction pattern corresponding to **a**. **c** HRTEM image at surface regions shows layered structures. **d** The fast Fourier transformation (FFT) and the inverse fast Fourier transformation (IFFT) images providing lattice fringes of **c**. **e** HRTEM image at surface regions shows spinel structures. **f** The FFT and IFFT images providing lattice fringes of **e**
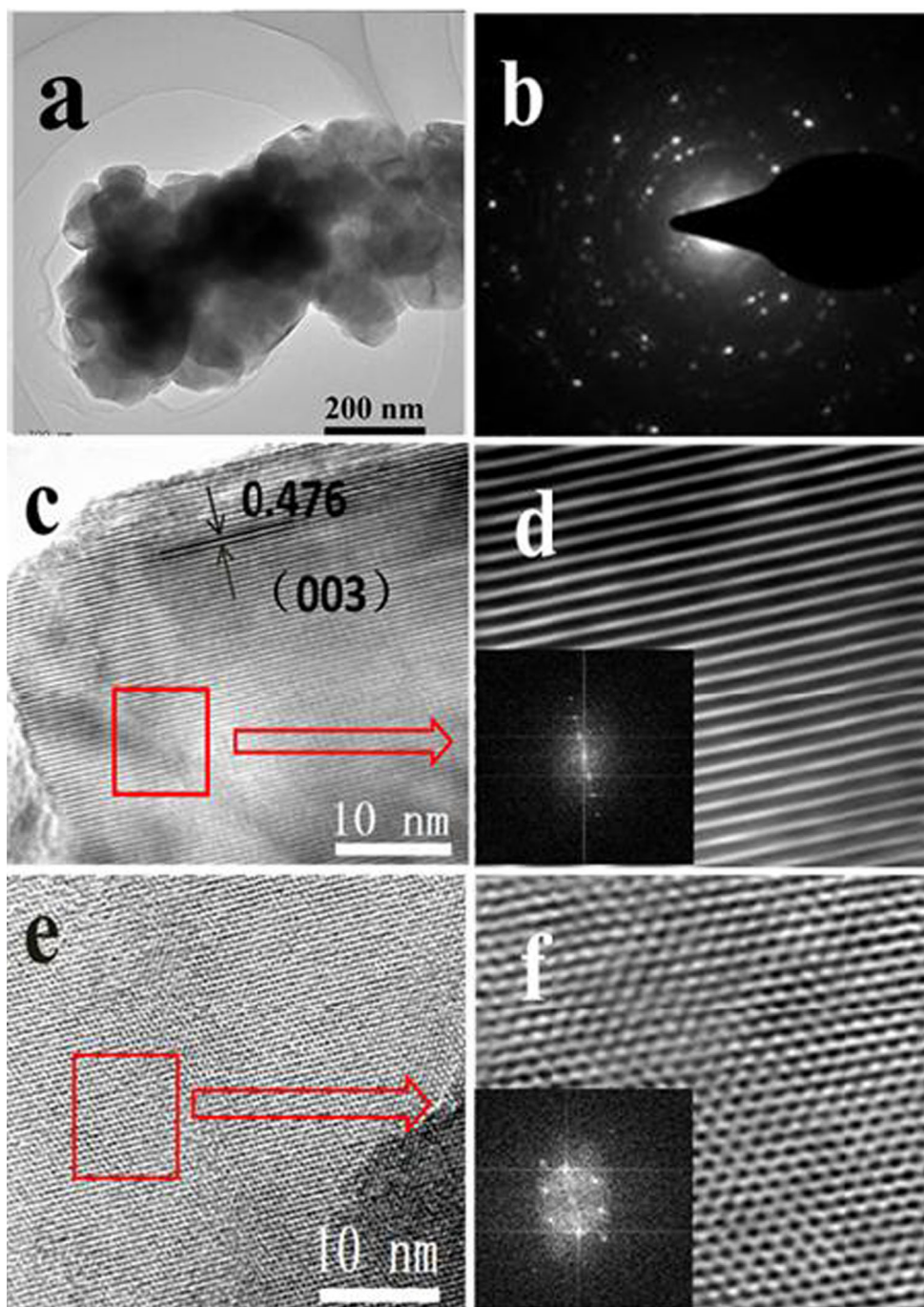
effect of particle size on electrochemical properties becomes obvious when the x value is above 0.05. There are two charge platforms at about 3.5 and 4.4 V which emerged only at the first cycle of these cathode materials. However, the first charge/discharge efficiency of all cathode materials is very low, only about 73 %. It has been reported [31] that because of the removal of Li_2O in the Li_2MnO_3 regions during the charging process, there is an inability to insert all of the lithium ions back into the lattice of cathode materials when discharging. A plateau appears at about 2.7 V in the discharge curve at (x=0.03, 0.05). Many people have studied this plateau [32–35]. They came to the conclusion that the insertion of lithium into the octahedral sites associated with the 2.7-V plateau. The degree of order and the particle size may be the dominant factor in determining the 2.7-V plateau length. The ordered phase, with the larger 16c sites, will fill with Li before the disordered phase. The small particle size, with a shorter distance for Li to diffuse, will make the insertion of Li easier. Therefore, the doped samples with lower cation disorder will have a longer plateau, but with the Mo content increased, the
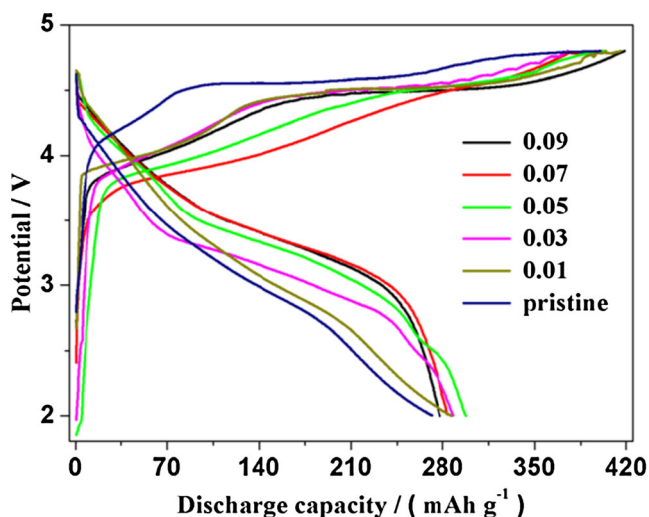
Fig. 4 The first charge/discharge curves of $Li_{1.2}Mn_{0.54}Co_{0.13}Ni_{0.13}O_2$ before and after doping with various amounts of Mo

particle size will get bigger resulting in the plateau getting shorter or even disappearing.

The rate capability is an important factor for battery performance. The normalized discharge capacity values are shown in Fig. 5. The specific discharge capacity of each sample gradually decreases with the increasing current density from 20 to 1,000 mA g^{-1}. The pristine sample decreases more sharply than the doped samples as the current density is increased to 200 mA g^{-1}. When the current density goes back to 20 mA g^{-1}, the 35th cycle discharge capacity returns to a high value. At each current density, the samples which are doped by Mo have higher capacity than the pristine. And with the increase of the content of Mo, the capacity first rises, peaks, then lowers. When x value is 0.05, the sample has a higher capacity than others at each current density. The doped samples have better rate capability than the pristine sample which may be because of the structure and the electronic conductivity. Beyond x level 0.05, the effect of the particles
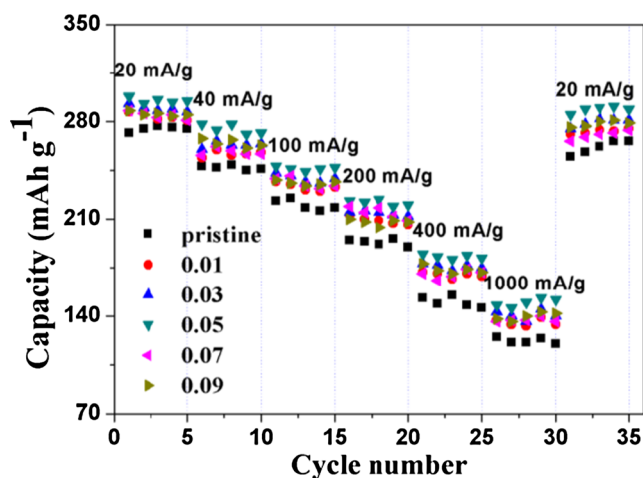
agglomeration on the rate capability becomes obvious, lowering the overall electrochemical properties level.

Figure 6 shows the average discharge voltage plots and coulombic efficiencies cycled at current density of 200 mA g^{-1} in the voltage range of 2.0~4.8 V. Compared with these samples, the average discharge voltage of the lightly doped (x=0.01, 0.03) and undoped samples are drastically reduced upon cycling, while the initial average discharge voltages of the heavy-doped (x>0.05) are much higher. This change in voltage is a straightforward indication of phase transformation. Mo doping may partially stabilize the local structure against transformation, thus maintaining and raising the average discharge voltage to a certain extent. The influence of surface side reactions on the electrochemical performance of as-prepared samples is explored based on the coulombic efficiencies. From the figure, all the coulombic efficiencies are low at first, and then increase with the cycle number, eventually leveling out at a high value of 95~100 %. The formation of a thick passivation layer (SEI film) on the surface of electrodes and the activation of Li_2MnO_3 in the first cycle are the reasons for the low coulombic efficiencies in the first cycles. The doped materials have high coulombic efficiencies, meaning that there are no additional side reactions after doping with Mo.

The cycling performance of the composite cathodes at current density of 200 mA g^{-1} in the voltage range of 2.0~4.8 V are shown in Fig. 7. During the extended cycling, the pristine delivered initial capacity values of 204 mAh g^{-1}, and have capacity retentions of 81.4 % after 100 cycles. The improved cathode materials have higher capacity. The highest capacity is 232.5 mAh g^{-1}, the corresponding x value is 0.05. The retentions of the improved cathode materials are higher than the pristine samples. It is therefore believed that the use of Mo resulted in better structural ordering and stability within the cathode materials thereby achieving high-capacity retentions.
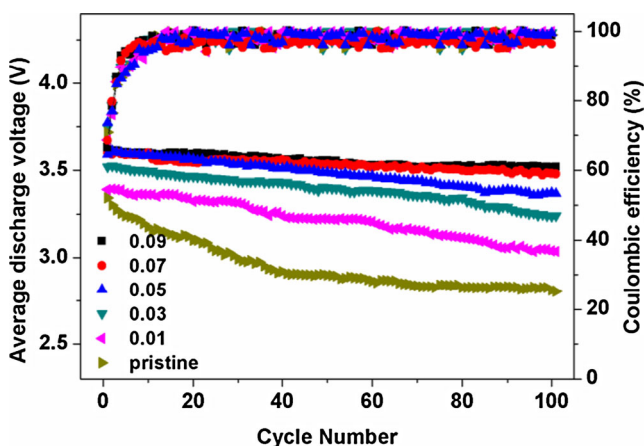

Fig. 5 The rate capability of $Li_{1.2}Mn_{0.54}Co_{0.13}Ni_{0.13}O_2$ before and after doping with various amounts of Mo

Fig. 6 The coulombic efficiencies and average discharge voltage of $Li_{1.2}Mn_{0.54}Co_{0.13}Ni_{0.13}O_2$ before and after doping with various amounts of Mo
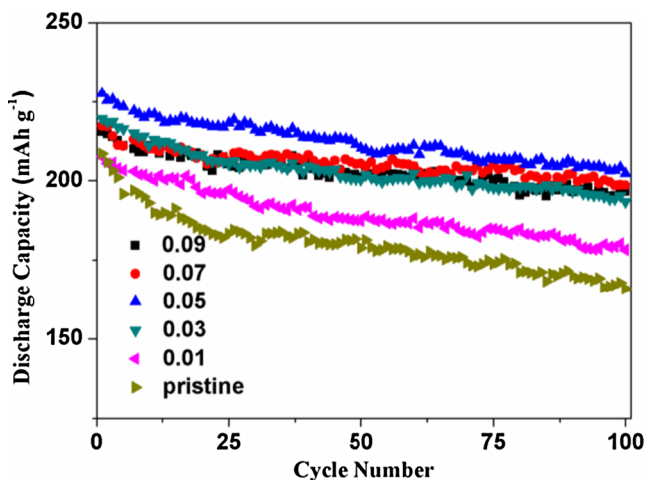
Fig. 7 The cycling performance of $Li_{1.2}Mn_{0.54}Co_{0.13}Ni_{0.13}O_2$ before and after doping with various amounts of Mo

AC EIS measurements of serial $Li_{1.2}Ni_{0.13-x}Co_{0.13}Mn_{0.54}Mo_xO_2$ electrodes of the initial cycle are shown in Fig. 8. As shown in Fig. 8, there is a semicircle in the high-frequency region and a slope line in the low-frequency region. The semicircle corresponds to an electrolyte–electrode interfacial resistance of charge transfer (Rct) and an interfacial capacitance(C) between the electrolyte and electrodes. The slope line corresponds to a Warburg impedance of lithium diffusion within the electrode and the electrolyte. The EIS spectra could be fitted with the equivalent circuit inserted in Fig. 8, which explains the impedance spectra through the electrolyte resistance R_S, and Warburg impedance of solid-phase diffusion (W) [36].

When the x value is 0, 0.01, 0.03, 0.05, 0.07, and 0.09, the working electrode possesses an approximate Rct value of 257, 151, 102, 88, 78, and 72 Ω. That is, for the serial $Li_{1.2}Mn_{0.54}Ni_{0.13+x}Co_{0.13}Mo_xO_2$ cathodes, their charge–transfer resistances decrease with increase of the content of Mo. It means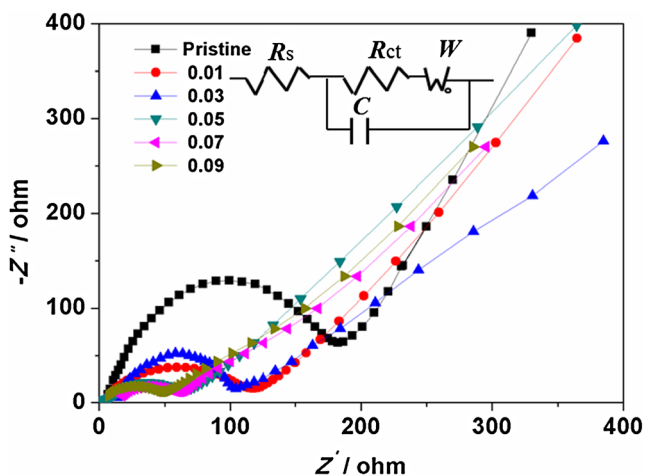 that the Mo doping obviously decreases the charge-transfer resistance, which further confirms that doping can improve the high rate performance. As reported [37, 38], EIS can be used to compare the electronic conductivity. The smaller charge-transfer resistance of Mo-doped $Li_{1.2}Mn_{0.54}Ni_{0.13}Co_{0.13}O_2$ indicates lithium ion transfer is easier than that of pristine $Li_{1.2}Mn_{0.54}Ni_{0.13}Co_{0.13}O_2$. This suggests the doped samples obtains or lose electrons easier. This might be the other reason why the cathode materials doped by Mo have better electrochemical properties.

Conclusions

The effects of doping Mo on the structure, morphology, and electrochemical performance of $Li_{1.2}Mn_{0.54}Ni_{0.13}Co_{0.13}O_2$ were investigated. It is shown that the capacity of the materials was obviously increased after doping the appropriate amount of Mo, it could deliver discharge capacities of 296.8 mAh g^{-1}, at a charge/discharge current density of 20 mA g^{-1} in the voltage range of 2.0–4.8 V. The structure and morphology of the doped samples are characterized and compared by the results of SEM and XRD. The doped samples have bigger lattice volume, and better layer structure ordering, but also have higher aggregation of particles, resulting in bigger particle size and worse electrochemical performance. The EIS results show that the doped samples obtain or lose electrons easier after doping. In this paper, the value of x is 0.05 is found to be the optimal amount of Mo.

References

1. Jafta CJ, Ozoemena KI, Mathe MK, Roos WD (2012) Synthesis, characterisation and electrochemical intercalation kinetics of nano-structured aluminium-doped $Li[Li_{0.2}Mn_{0.54}Ni_{0.13}Co_{0.13}]O_2$ cathode material for lithium ion battery. Electrochim Acta 85:411–422
2. Singh G, West WC, Soler J, Katiyar RS (2012) In situ Raman spectroscopy of layered solid solution Li_2MnO_3–$LiMO_2$ (M=Ni, Mn, Co). J Power Sources 218:34–38
3. West W, Soler J, Ratnakumar B (2012) Preparation of high quality layered-layered composite Li_2MnO_3–$LiMO_2$(M=Ni, Mn, Co) Li-ion cathodes by a ball milling–annealing process. J Power Sources 204:200–204
4. Yang S, Huang G, Hu S, Hou X, Huang Y, Yue M, Lei G (2014) Improved electrochemical performance of the $Li_{1.2}Ni_{0.13}Co_{0.13}Mn_{0.54}O_2$ wired by CNT networks for lithium-ion batteries. Mater Lett 118:8–11
5. Zhao C, Wang X, Liu X, Zhang H, Shen Q (2014) Mn–Ni content-dependent structures and electrochemical behaviors of serial $Li_{1.2}Ni_{0.13+x}Co_{0.13}Mn_{0.54-x}O2$ as lithium-ion battery cathodes. ACS Appl Mater Interfaces 6:2386–2392

Fig. 8 Nyquist plots of $Li_{1.2}Mn_{0.54}Co_{0.13}Ni_{0.13}O_2$ before and after doping with various amounts of Mo

6. Li Q, Li G, Fu C, Luo D, Fan J, Li L (2014) K^+-doped $Li_{1.2}Mn_{0.54}Co_{0.13}Ni_{0.13}O_2$: a novel cathode material with an enhanced cycling stability for lithium-ion batteries. ACS Appl Mater Interfaces 6:10330–10341

7. Song B, Liu H, Liu Z, Xiao P, Lai MO, Lu L (2013) High rate capability caused by surface cubic spinels in Li-rich layer-structured cathodes for Li-ion batteries. Sci Rep 3:3094

8. Zheng J, Wu X, YANG Y (2011) A comparison of preparation method on the electrochemical performance of cathode material Li$[Li_{0.2}Mn_{0.54}Ni_{0.13}Co_{0.13}]O_2$ for lithium ion battery. Electrochim Acta 56:3071–3078

9. Gao J, Kim J, Manthiram A (2009) High capacity Li$[Li_{0.2}Mn_{0.54}Ni_{0.13}Co_{0.13}]O_2$–$V_2O_5$ composite cathodes with low irreversible capacity loss for lithium ion batteries. Electrochem Commun 11:84–86

10. Lee E-S, Manthiram A (2014) Smart design of lithium-rich layered oxide cathode compositions with suppressed voltage decay. J Mater Chem 2:3932–3939

11. Cong L-N, Gao X-G, Ma S-C, Guo X, Zeng Y-P, Tai L-H, Wang R-S, Xie H-M et al (2014) Enhancement of electrochemical performance of Li$[Li_{0.2}Mn_{0.54}Ni_{0.13}Co_{0.13}]O_2$ by surface modification with $Li_4Ti_5O_{12}$. Electrochim Acta 115:399–406

12. Wu F, Wang Z, Su Y, Yan N, Bao L, Chen S (2014) Li$[Li_{0.2}Mn_{0.54}Ni_{0.13}Co_{0.13}]O2$–$MoO3$ composite cathodes with low irreversible capacity loss for lithium ion batteries. J Power Sources 247:20–25

13. Li L, Zhang X, Chen R, Zhao T, Lu J, Wu F, Amine K (2014) Synthesis and electrochemical performance of cathode material Li1.2Co0.13Ni0.13Mn0.54O2 from spent lithium-ion batteries. J Power Sources 249:28–34

14. Whitfield P, Davidson I, Cranswick L, Swainson I, Stephens P (2005) Investigation of possible superstructure and cation disorder in the lithium battery cathode material LiMn< sub> 1/3</sub> Ni< sub> 1/3</sub> Co< sub> 1/3</sub> O< sub> 2</sub> using neutron and anomalous dispersion powder diffraction. Solid State Ionics 176:463–471

15. Zheng J, Wu X, Yang Y (2013) Improved electrochemical performance of Li$[Li_{0.2}Mn_{0.54}Ni_{0.13}Co_{0.13}]O_2$ cathode material by fluorine incorporation. Electrochim Acta 105:200–208

16. Du K, Yang F, G-r H, Z-d P, Y-b C, Ryu KS (2013) Sodium additive to improve rate performance of Li $Li_{0.2}Mn_{0.54}Ni_{0.13}Co_{0.13}$ O_2 material for Li-ion batteries. J Power Sources 244:29–34

17. Park J-H, Lim J, Yoon J, Park K-S, Gim J, Song J, Park H, Im D et al (2012) The effects of Mo doping on 0.3Li$[Li_{0.33}Mn_{0.67}]O_2$·0.7Li$[Ni_{0.5}Co_{0.2}Mn_{0.3}]O_2$ cathode material. Dalton Trans 41:3053–3059

18. Takahashi Y, Kijima N, Hayakawa H, Awaka J, Akimoto J (2008) Single-crystal synthesis and structure refinement of Li_2MoO_3. J Phys Chem Solids 69:1518–1520

19. Wu F, Tian J, Su Y, Guan Y, Jin Y, Wang Z, He T, Bao L et al (2014) Lithium-active molybdenum trioxide coated $LiNi_{0.5}Co_{0.2}Mn_{0.3}O_2$ cathode material with enhanced electrochemical properties for lithium-ion batteries. J Power Sources 269:747–754

20. Gao Y, Ma J, Wang X, Lu X, Bai Y, Wang Z, Chen L (2014) Improved electron/Li-ion transport and oxygen stability of Mo-doped Li_2MnO_3. J Mater Chem 2:4811–4818

21. Konishi H, Yoshikawa M, Hirano T (2013) The effect of thermal stability for high-Ni-content layer-structured cathode materials, $LiNi_{0.8}Mn_{0.1-x}Co_{0.1}Mo_xO_2$ ($x=0$, 0.02, 0.04). J Power Sources 244:23–28

22. Jiang K-C, Xin S, Lee J-S, Kim J, Xiao X-L, Guo Y-G (2012) Improved kinetics of $LiNi_{1/3}Mn_{1/3}Co_{1/3}O_2$ cathode material through reduced graphene oxide networks. Phys Chem Chem Phys 14:2934–2939

23. Wang J, Yao XY, Zhou XF, Liu ZP (2011) Synthesis and electrochemical properties of layered lithium transition metal oxides. J Mater Chem 21:2544–2549

24. Bai Y, Wang X, Zhang X, Shu H, Yang X, Hu B, Wei Q, Wu H et al (2013) The kinetics of Li-ion deintercalation in the Li-rich layered $Li_{1.12}[Ni_{0.5}Co_{0.2}Mn_{0.3}]0.89O_2$ studied by electrochemical impedance spectroscopy and galvanostatic intermittent titration technique. Electrochim Acta 109:355–364

25. Liu JL, Chen L, Hou MY, Wang F, Che RC, Xia YY (2012) General synthesis of xLi_2MnO_3·$_{1-x}LiMn_{1/3}Ni_{1/3}Co_{1/3}O_2$ nanomaterials by a molten-salt method: towards a high capacity and high power cathode for rechargeable lithium batteries. J Mater Chem 22:25380–25387

26. Zhao TL, Chen S, Li L, Zhang XF, Chen RJ, Belharouak I, Wu F, Amine K (2013) Synthesis, characterization, and electrochemistry of cathode material Li$[Li_{0.2}Co_{0.13}Ni_{0.13}Mn_{0.54}]O_2$ using organic chelating agents for lithium-ion batteries. J Power Sources 228:206–213

27. Wang Q, Huo J, Zheng Y, Pang S, He Z (2013) Design of red/green emissive lanthanide activated nano-materials by supersonic and microwave co-irradiations. Opt Mater 35:1146–1150

28. Cho T-H, Shiosaki Y, Noguchi H (2006) Preparation and characterization of layered $LiMn_{1/3}Ni_{1/3}Co_{1/3}O_2$ as a cathode material by an oxalate co-precipitation method. J Power Sources 159:1322–1327

29. Xiao J, Chernova NA, Whittingham MS (2008) Layered mixed transition metal oxide cathodes with reduced cobalt content for lithium ion batteries. Chem Mater 20:7454–7464

30. Dorset DL, Siskin M (2008) Molecular assemblies in asphaltenes and their high-temperature coke products. Part 1: initial molecular organization. Energy Fuels 22:2512–2517

31. Yu S-H, Yoon T, Mun J, Park S, Kang Y-S, Park J-H, Oh SM, Sung Y-E (2013) Continuous activation of Li_2MnO_3 component upon cycling in $Li_{1.167}Ni_{0.233}Co_{0.100}Mn_{0.467}Mo_{0.033}O_2$ cathode material for lithium ion batteries. J Mater Chem 1:2833–2839

32. Johnson CS, Li N, Lefief C, Vaughey JT, Thackeray MM (2008) Synthesis, characterization and electrochemistry of lithium battery electrodes: xLi_2MnO_3·$_{(1-x)}LiMn_{0.333}Ni_{0.333}Co_{0.333}O_2$ ($0 \leq x \leq 0.7$). Chem Mater 20:6095–6106

33. Moorhead-Rosenberg Z, Chemelewski KR, Goodenough JB, Manthiram A (2013) Magnetic measurements as a viable tool to assess the relative degrees of cation ordering and Mn_{3+} content in doped $LiMn_{1.5}Ni_{0.5}O_4$ spinel cathodes. J Mater Chem 1:10745–10752

34. Liu W, Fang G, Xia B, Sun H, Kaneko S, Li D (2013) Improved electrochemical properties of Li$[Li_{0.2}Ni_{0.17}Mn_{0.56}Co_{0.07}]O_2$ cathode material via micro-structural rearrangement. RSC Adv 3:15630–15635

35. Uzun D, Doğrusöz M, Mazman M, Biçer E, Avci E, Şener T, Kaypmaz TC, Demir-Cakan R (2013) Effect of MnO_2 coating on layered Li($Li_{0.1}Ni_{0.3}Mn_{0.5}Fe_{0.1}$)$O_2$ cathode material for Li-ion batteries. Solid State Ionics 249–250:171–176

36. Wang GG, Wang JM, Mao WQ, Shao HB, Zhang JQ, Cao CN (2005) Physical properties and electrochemical performance of $LiMn_2O_4$ cathode materials prepared by a precipitation method. J Solid State Electrochem 9:524–530

37. Lee J, Kumar P, Moudgil BM, Singh RK (2013) Electrochemical enhancement of $LiFePO_4$ as a cathode material by incorporating Cu flakes for lithium ion rechargeable battery. Solid State Ionics 231:18–24

38. Zhang QY, Zhang CL, Li B, Jiang DD, Kang SF, Li X, Wang YG (2013) Preparation and characterization of W-doped $Li_4Ti_5O_{12}$ anode material for enhancing the high rate performance. Electrochim Acta 107:139–146